Supplementary Information (SI)

Atmospheric ice-nucleating particles in the Eastern Mediterranean and the potential influence of fertile soils

Mark D. Tarn[1], Bethany V. Wyld[1], Naama Reicher[2], Matan Alayof[2], Daniella Gat[2], Alberto Sanchez-Marroquin[1], Sebastien N. F. Sikora[1], Alexander D. Harrison[1], Yinon Rudich[2], Benjamin J. Murray[1]

[1]School of Earth and Environment, University of Leeds, Leeds, LS2 9JT, United Kingdom
[2]Department of Earth and Planetary Sciences, Weizmann Institute of Science, Rehovot 76100, Israel

Correspondence to: Mark D. Tarn (m.d.tarn@leeds.ac.uk), Benjamin J. Murray (b.j.murray@leeds.ac.uk)

Contents

1 Aerosol sampling details

Table S1: Details of the aerosol samples collected during the field campaign in Rehovot, Israel, in October-November 2018. Samples were either collected using a filter-based platform (BGI PQ100 Air Sampling System with a PM_{10} inlet, Mesa Laboratories), or using an impinger (Coriolis® Micro, Bertin Technologies), then the particle suspended in purified water of a known volume (i.e. the wash volume). All times are local, and dates are provided in the DD/MM/YY format.

Date (DD/MM/YY)	Start time	End time	Sampling time (min)	Sampling rate (L min^{-1})	Volume of sampled air (L)	Wash volume (mL)	Sampling method
3 h filter (PQ100) samples							
25/10/18	10:10	11:10	60	16.66	1,000	4	Filter-based
25/10/18	15:07	18:10	183	16.66	3,049	4	Filter-based
26/10/18	12:09	15:17	188	16.66	3,132	4	Filter-based
26/10/18	15:40	18:40	180	16.66	2,999	4	Filter-based
27/10/18	10:20	13:20	180	16.66	2,999	4	Filter-based
27/10/18	15:18	18:18	180	16.66	2,999	4	Filter-based
28/10/18	09:28	12:28	180	16.66	2,999	4	Filter-based
28/10/18	14:49	17:49	180	16.66	2,999	4	Filter-based
29/10/18	09:42	12:42	180	16.66	2,999	4	Filter-based
29/10/18 (PM_{10} and PM_1)	13:58	16:58	180	16.66	2,999	4	Filter-based
30/10/18	06:00	09:00	180	16.66	2,999	4	Filter-based
30/10/18	09:37	12:37	180	16.66	2,999	4	Filter-based
30/10/18	13:13	16:13	180	16.66	2,999	4	Filter-based
31/10/18	09:38	12:38	180	16.66	2,999	4	Filter-based
31/10/18	14:28	17:28	180	16.66	2,999	4	Filter-based
01/11/18	09:47	12:47	180	16.66	2,999	4	Filter-based

01/11/18	14:55	17:55	180	16.66	2,999	4	Filter-based
02/11/18	10:24	13:24	180	16.66	2,999	4	Filter-based
02/11/18	14:36	17:36	180	16.66	2,999	4	Filter-based
03/11/18	09:34	12:34	180	16.66	2,999	4	Filter-based
03/11/18	14:08	17:08	180	16.66	2,999	4	Filter-based
24 h filter (PQ100) samples							
25/10/18 to 26/10/18	11:45 (25/10/18)	11:45 (26/10/18)	1,440	16.66	23,990	4	Filter-based
26/10/18 to 27/10/18	11:58 (26/10/18)	11:58 (27/10/18)	1,440	16.66	23,990	4	Filter-based
27/10/18 to 28/10/18	12:20 (27/10/18)	12:20 (28/10/18)	1,440	16.66	23,990	4	Filter-based
28/10/18 to 29/10/18	11:58 (28/10/18)	05:29 (29/10/18)	1,051	16.66	17,510	4	Filter-based
Impinger (Coriolis) samples							
26/10/18	(1) 11:21 (2) 11:37 (3) 11:50 (4) 12:08 (5) 12:19 (6) 12:30	(1) 11:31 (2) 11:47 (3) 12:00 (4) 12:18 (5) 12:29 (6) 12:40	60	100	6,000	6.64	Impinger-based
27/10/18	(1) 15:36 (2) 15:53	(1) 15:46 (2) 16:03	20	300	6,000	9.61	Impinger-based
28/10/18	(1) 15:00 (2) 15:19	(1) 15:10 (2) 15:29	20	300	6,000	4.73	Impinger-based
29/10/18	(1) 15:32 (2) 15:48	(1) 15:42 (2) 15:58	20	300	6,000	4.87	Impinger-based
30/10/18	(1) 16:11 (2) 16:25	(1) 16:21 (2) 16:35	20	300	6,000	4.80	Impinger-based
02/11/18	(1) 15:16 (2) 15:38	(1) 15:26 (2) 15:48	20	300	6,000	5.91	Impinger-based
03/11/18	(1) 15:09 (2) 15:23	(1) 15:19 (2) 15:33	20	300	6,000	4.99	Impinger-based

Table S2: Classification of air mass trajectory categories as per Gat et al. (2021), which was part of the same field campaign. Days with dust events are identified with a subscript "$_D$", and were trajectories were identified as dust events if the PM_{10} loading exceeded 44 µg m^{-3} (Krasnov et al., 2016; Gat et al. 2021). More information about the wind directions and speeds throughout the campaign are provided in Figure 2e in the main paper, while air mass back trajectories are shown in Figure S17 in the SI. Dates are in the DD/MM/YY format.

Air mass trajectory	ID	Dates (DD/MM/YY)
Southwesterly with Saharan dust event	SW_D	25/10/18
Northwesterly	NW	26/10/18 – 27/10/18
Easterly with Syrian and/or Arabian dust event	E_D	28/10/18 – 31/10/18
Easterly	E	01/11/18 – 03/11/18

Table S3: Details of particle concentrations of the aerosol samples, including particle number concentration (d*N*), mass concentration of particulate matter less than 10 µm in diameter (PM_{10}), and particle surface area (d*S*). Data for the filter-based samples (see Table S1) are for PM_{10} since the PQ100 filter sampler used a PM_{10} inlet head. Air mass category IDs are given in Table S2. All times are local, and dates are in the DD/MM/YY format.

Date (DD/MM/YY)	Start time	End time	Sample designation	Average particle concentration, d*N* (cm^{-3})	Average PM_{10} value (µg m^{-3})	Average particle surface area concentration, d*S* (µm^2 cm^{-3})	Air mass category and ID
3 h filter (PQ100) samples							
25/10/18	10:10	11:10	181025 morning	507 ± 95	268 ± 253	773 ± 373	SW_D
25/10/18	15:07	18:10	181025 afternoon	357 ± 119	332 ± 110	845 ± 211	SW_D
26/10/18	12:09	15:17	181026 morning	46 ± 6	18 ± 9	103 ± 54	NW1
26/10/18	15:40	18:40	181026 afternoon	61 ± 9	21 ± 7	119 ± 11	NW1
27/10/18	10:20	13:20	181027 morning	33 ± 6	9 ± 3	97 ± 13	NW2
27/10/18	15:18	18:18	181027 afternoon	53 ± 6	14 ± 7	193 ± 25	NW2
28/10/18	09:28	12:28	181028 morning	73 ± 20	76 ± 33	229 ± 45	E_D1
28/10/18	14:49	17:49	181028 afternoon	82 ± 15	90 ± 18	301 ± 46	E_D1
29/10/18	09:42	12:42	181029 morning	119 ± 21	87 ± 15	279 ± 39	E_D2
29/10/18 (PM_{10} and PM_1)	13:58	16:58	181029 afternoon	136 ± 13	99 ± 13	326 ± 39	E_D2
30/10/18	06:00	09:00	181030 early morning	208 ± 14	130 ± 10	349 ± 21	E_D3
30/10/18	09:37	12:37	181030 morning	175 ± 6	113 ± 8	358 ± 16	E_D3

30/10/18	13:13	16:13	181030 afternoon	151 ± 16	94 ± 10	314 ± 30	E_D3
31/10/18	09:38	12:38	181031 morning	142 ± 7	68 ± 7	270 ± 13	E_D4
31/10/18	14:28	17:28	181031 afternoon	165 ± 7	91 ± 28	325 ± 38	E_D4
01/11/18	09:47	12:47	181101 morning	88 ± 7	55 ± 25	239 ± 37	E1
01/11/18	14:55	17:55	181101 afternoon	106 ± 20	77 ± 19	310 ± 61	E1
02/11/18	10:24	13:24	181102 morning	100 ± 17	47 ± 92	243 ± 112	E2
02/11/18	14:36	17:36	181102 afternoon	107 ± 10	46 ± 9	269 ± 20	E2
03/11/18	09:34	12:34	181103 morning	196 ± 27	36 ± 16	275 ± 32	E3
03/11/18	14:08	17:08	181103 afternoon	180 ± 14	35 ± 6	302 ± 19	E3
24 h filter (PQ100) samples							
25/10/18 to 26/10/18	11:45 (25/10/18)	11:45 (26/10/18)	181025 to 181026 (24 h)	-	-	-	SW_D/NW1
26/10/18 to 27/10/18	11:58 (26/10/18)	11:58 (27/10/18)	181026 to 181027 (24 h)	-	-	-	NW1/NW2
27/10/18 to 28/10/18	12:20 (27/10/18)	12:20 (28/10/18)	181027 to 181028 (24 h)	-	-	-	NW2/E_D1
28/10/18 to 29/10/18	11:58 (28/10/18)	05:29 (29/10/18)	181028 to 181029 (17.5 h)	-	-	-	E_D2/E_D3
Impinger (Coriolis) samples-							
26/10/18	11:21	12:40	181026 morning (impinger)	53 ± 10	19 ± 5	103 ± 18	NW1

27/10/18	15:36	16:03	181027 afternoon (impinger)	47 ± 3	13 ± 6	167 ± 13	NW2
28/10/18	15:00	15:29	181028 afternoon (impinger)	67 ± 3	91 ± 12	287 ± 21	E_D1
29/10/18	15:32	15:58	181028 afternoon (impinger)	150 ± 6	108 ± 8	352 ± 15	E_D2
30/10/18	16:11	16:35	181030 afternoon (impinger)	171 ± 8	117 ± 25	394 ± 50	E_D3
02/11/18	15:16	15:48	181102 afternoon (impinger)	108 ± 6	43 ± 6	273 ± 16	E2
03/11/18	15:09	15:33	181102 afternoon (impinger)	161 ± 8	31 ± 3	286 ± 12	E3

2 Size-resolved biological analysis

Table S4: List of the quantitative Polymerase Chain Reaction (qPCR) primers used for the determination of total bacterial and total fungal airborne concentrations. 16S ribosomal RNA was used for bacterial analysis, while nuclear ribosomal internal transcribed spacer (ITS) was used for fungal analysis.

Target gene	Primers	Sequence	Reference
16S ribosomal RNA (bacteria)	331F	TCCTACGGGAGGCAGCAGT	Bräuer et al., 2011
	518R	ATTACCGCGGCTGCTGG	
ITS (fungi)	ITS1F	CTTGGTCATTTAGAGGAAGTAA	White et al., 1990
	ITS2R	GCTGCGTTCTTCATCGATGC	

3 Fraction frozen curves for blank measurements

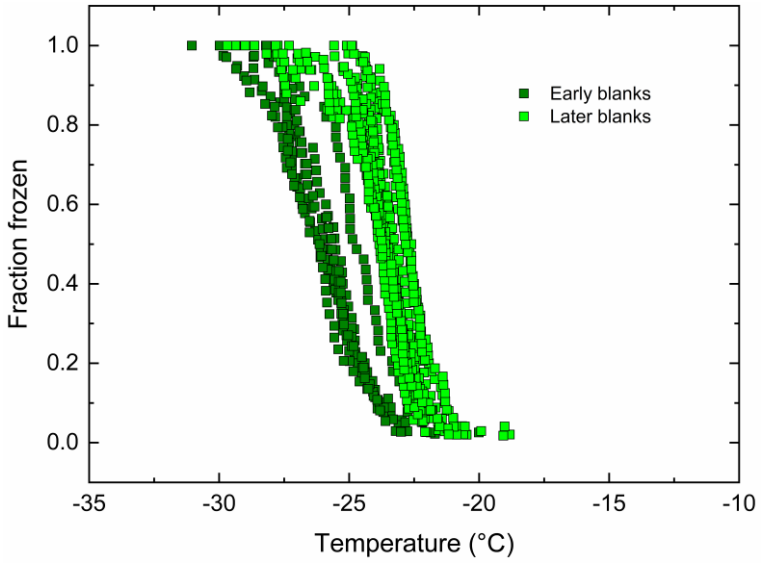

Figure S1: Plot showing the fraction frozen curves of all of the purified water blanks analysed during the field campaign in the Eastern Mediterranean using the Microlitre Nucleation by Immersed Particle Instrument (µL-NIPI) droplet freezing assay. The blanks are separated into two categories since the quality of the blanks changed suddenly during the campaign. "Early blanks" refers to those measured from 25/10/18 (DD/MM/YY) to 30/10/18. "Later blanks" refers to those measured between 31/10/18 and 04/11/18. The later blanks froze at slightly warmer temperatures than the early blanks.

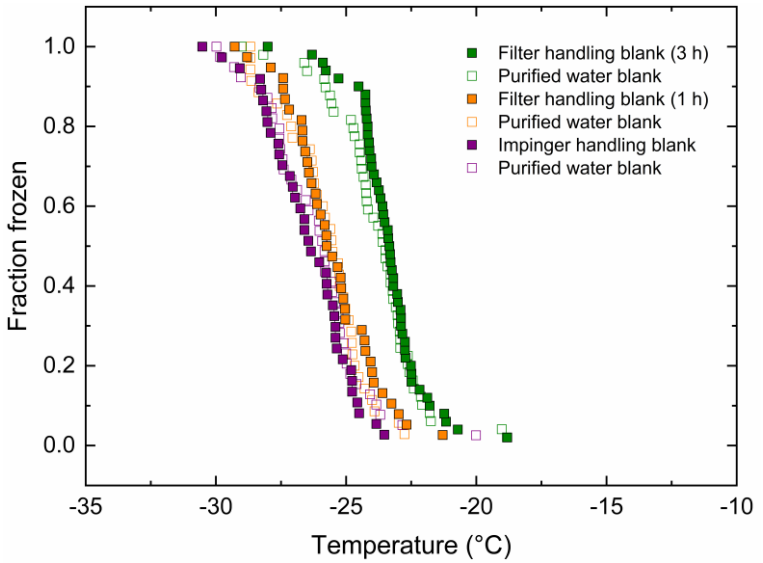

Figure S2: Fraction frozen curves showing the handling blanks from the BGI PQ100 filter system and the Coriolis® Micro impinger system versus purified water blanks that used the same water as in the handling blanks. Filter handling blanks were collected by sampling air through a HEPA (high-efficiency particulate air) filter and onto a polycarbonate track-etched membrane filter (1.0 µm pore size, 47 mm diameter, Whatman® Nuclepore™) using a Mesa Labs BGI PQ100 Air Sampling System. Two membrane filters were collected for handling blank tests: one for 1 hour of sampling through the HEPA filter (collected on 25/10/18, so compared to one of the "early" blanks), and one for 3 hours of sampling through the HEPA filter (collected on 03/11/18, so compared to one of the blanks in the "later" set). The filters were then washed with water, which was subsequently analysed using the µL-NIPI droplet freezing assay technique. The Coriolis impinger handling blank (collected on 27/10/18, so compared to one of the "early" blanks) was obtained by filling a sampling cone with water, attaching it to the impinger, then removing it and analysing the water via the µL-NIPI; no air was sampled into the cone due to the shape of the impinger inlet making it difficult to from a seal with a HEPA filter. The results show no discernible differences between the handling blanks and the purified water blanks.

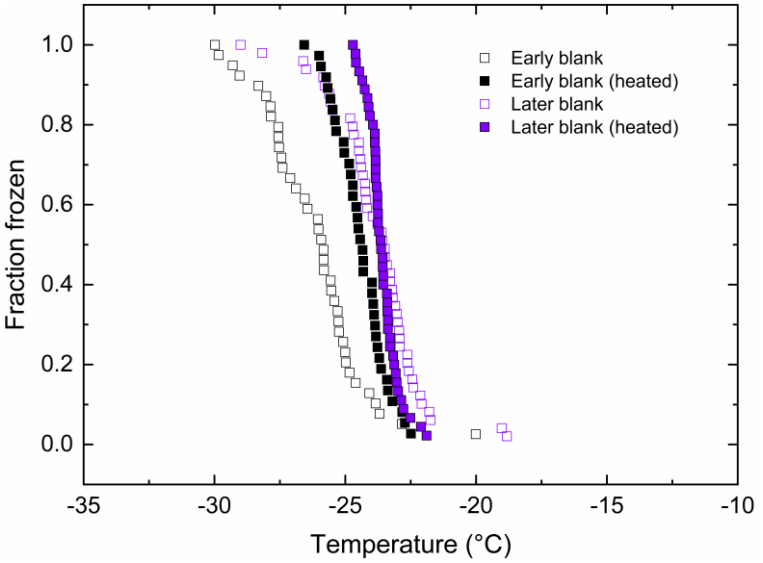

Figure S3: Plot showing the effect of heating on purified water blanks as a control for the sample heating tests. Examples are shown for an "early" blank (27/10/18) and a "later" blank (03/11/18) due to the change in characteristics of the blanks partway through the campaign.

4 Fraction frozen curves for aerosol samples

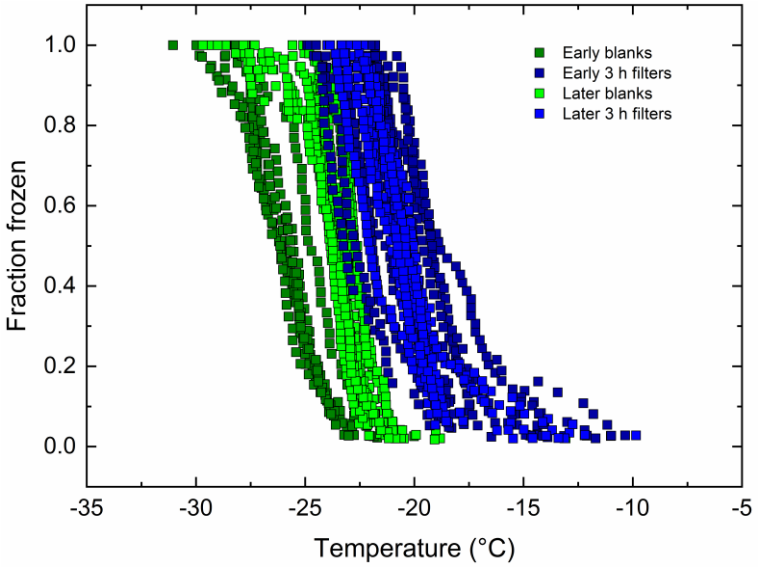

Figure S4: Fraction frozen curves for all of the aerosol samples collected onto filters for 3 h via the BGI PQ100 Air Sampling System and analysed using the µL-NIPI droplet freezing assay. The blanks and samples are separated into categories of "Early" (25/10/18 to 30/10/18) and "Later" (31/10/18 to 04/11/18) due to the quality of the blanks changing on 31/10/18, hence the samples collected during one time period can be compared correctly with the blanks from that same period.

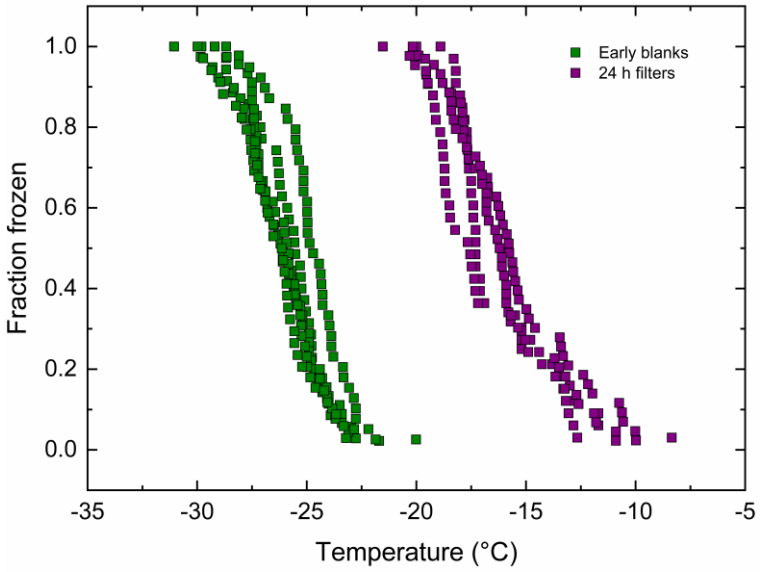

Figure S5: Fraction frozen curves for all 24 h filter-based samples collected using the BGI PQ100 Air Sampling System and analysed using the µL-NIPI droplet freezing assay. The 24 h samples were only collected prior to the change in quality of the purified water blanks partway through the campaign, hence only the "Early" blanks are shown against the aerosol samples.

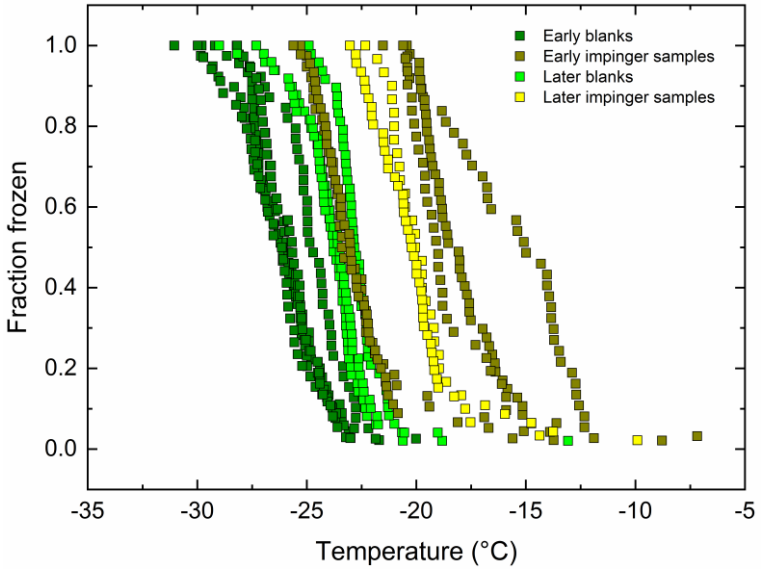

Figure S6: Fraction frozen curves for all aerosol samples collected using the Coriolis® Micro impinger system for 20-60 min and analysed using the µL-NIPI droplet freezing assay. The blanks and samples are separated into categories of "Early" (25/10/18 to 30/10/18) and "Later" (31/10/18 to 04/11/18) due to the quality of the blanks changing on 31/10/18, hence the samples collected during one time period can be compared correctly with the blanks from that same period.

5 Fraction frozen curves for heat treated aerosol samples

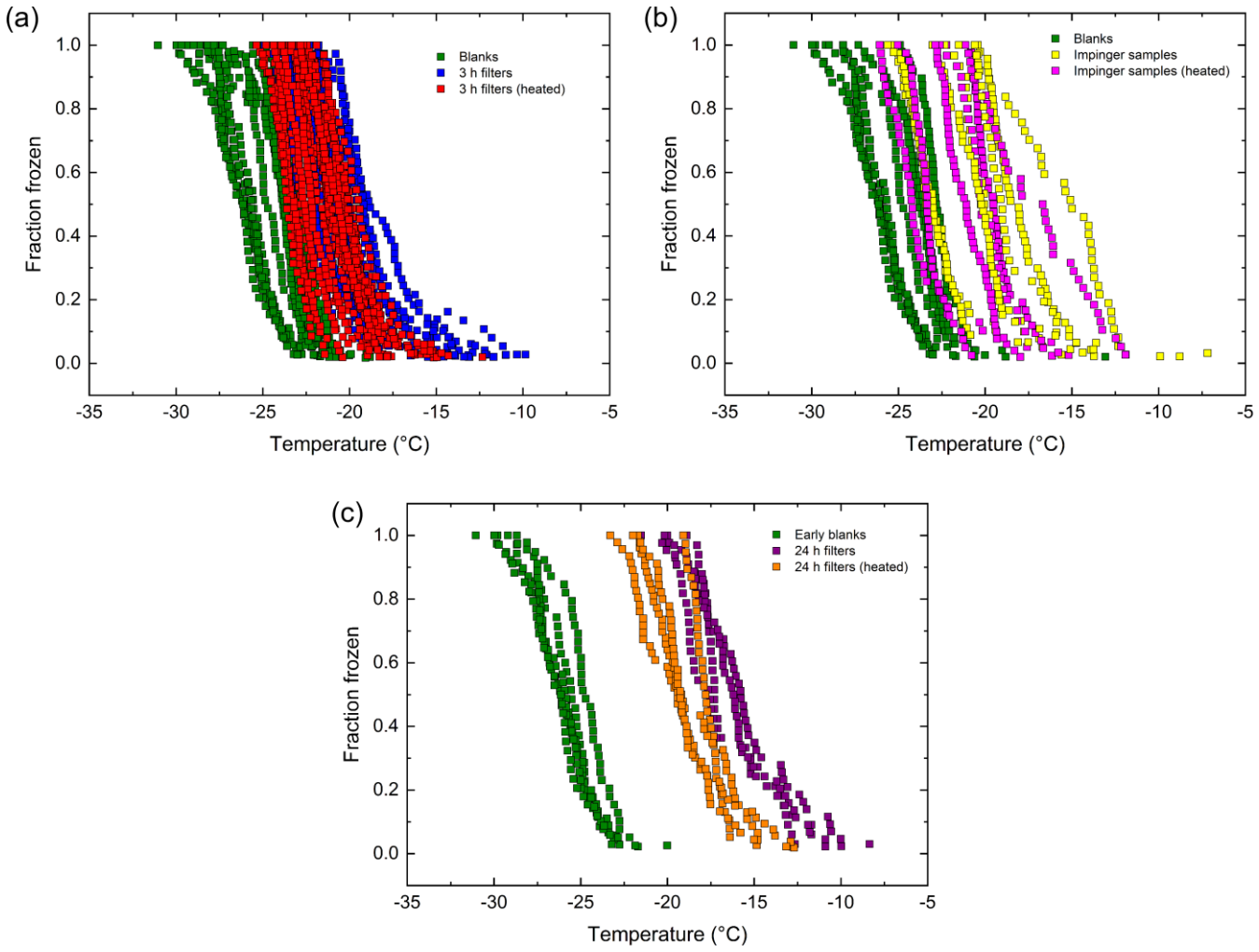

Figure S7: Fraction frozen curves for heat treated and unheated aerosol samples (a) 3 h filter samples, (b) Coriolis impinger samples, and (c) 24 h filter samples.

6 Background subtractions of INP spectra

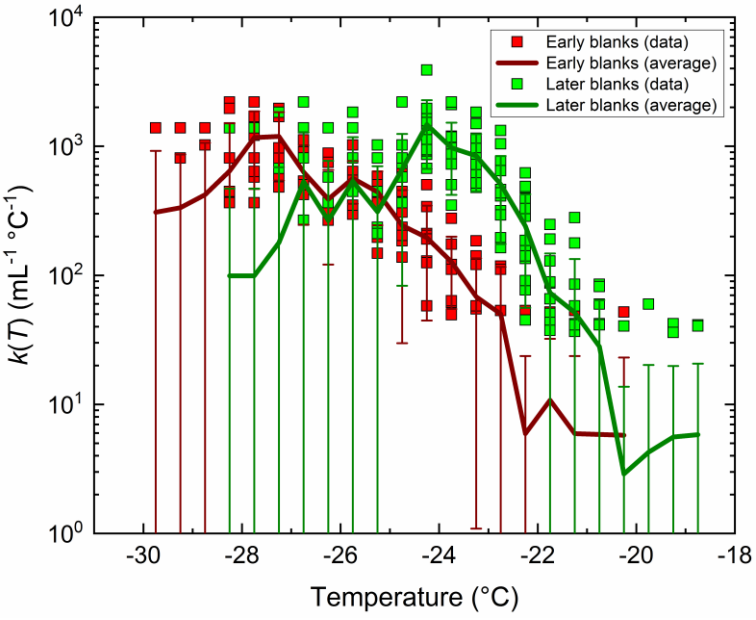

Figure S8: Blank data binned into 0.5 °C temperature intervals and represented in terms of the differential freezing nucleus spectrum, $k(T)$, as described by Vali (2019) and by Harrison et al. (2022). Data are shown separately for the "early" blanks (in red) and the "later" blanks (in green). The two sets of blanks were each averaged and these are shown represented by lines together with standard deviations. These average values were later subtracted from the ice nucleation data from the aerosol samples.

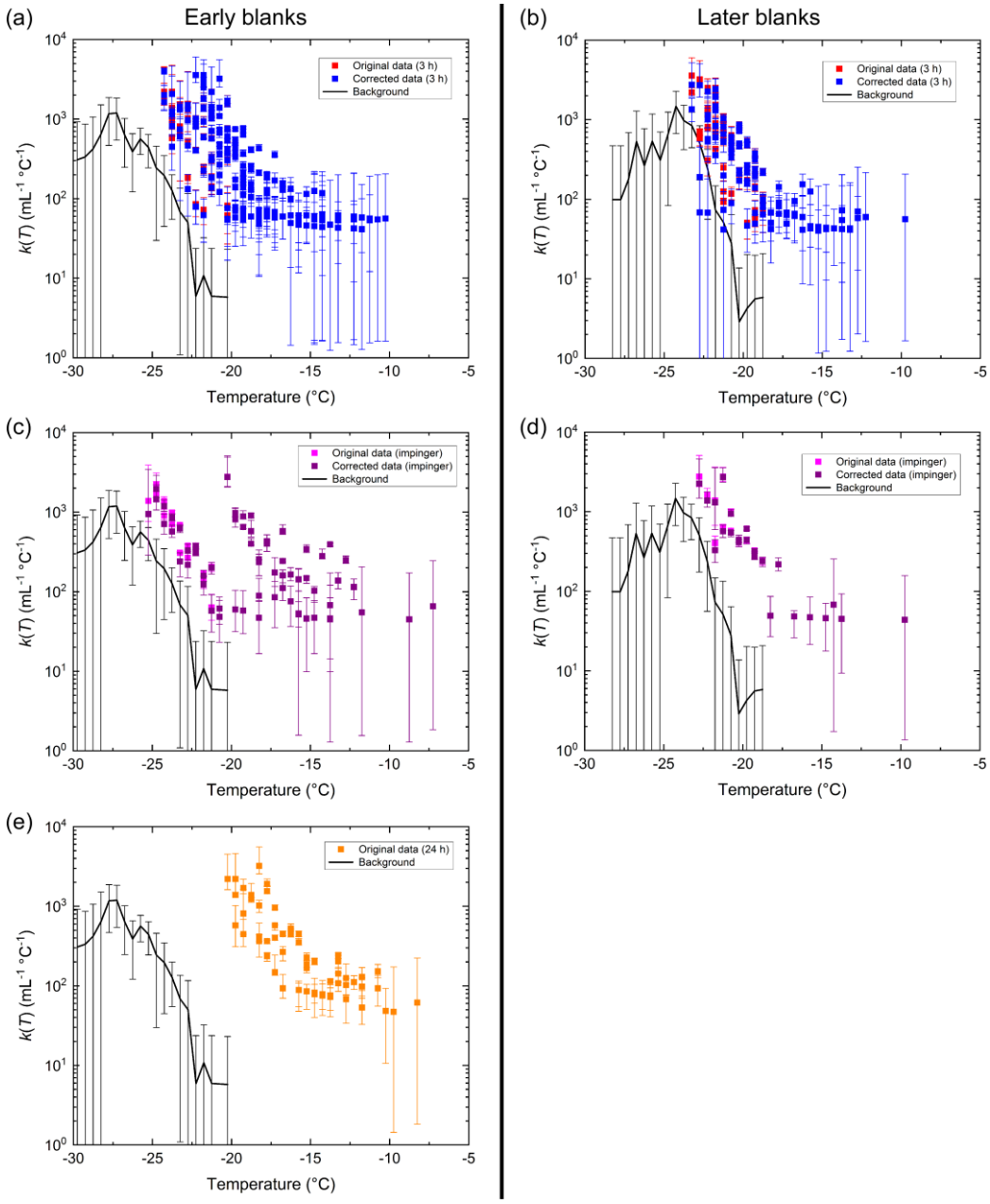

Figure S9: Sample data binned into 0.5 °C temperature intervals and represented in terms of the differential freezing nucleus spectrum, *k*(*T*), as per Vali (2019) and Harrison et al. (2022). The plots show original and background-subtracted data for (a) 3 h filter samples during the "early blanks" period of time, (b) 3 h filter samples during the "later blanks" period of time, (c) impinger samples during the "early blanks" period of time, (d) impinger samples during the "later blanks" period of time, (e) 24 h filter samples during the "early blanks" period of time. Background-subtracted sample values would next be converted to the cumulative ice-active site volume density, *K*(*T*), by summing the background-subtracted sample *k*(*T*) values for temperatures warmer than *T*.

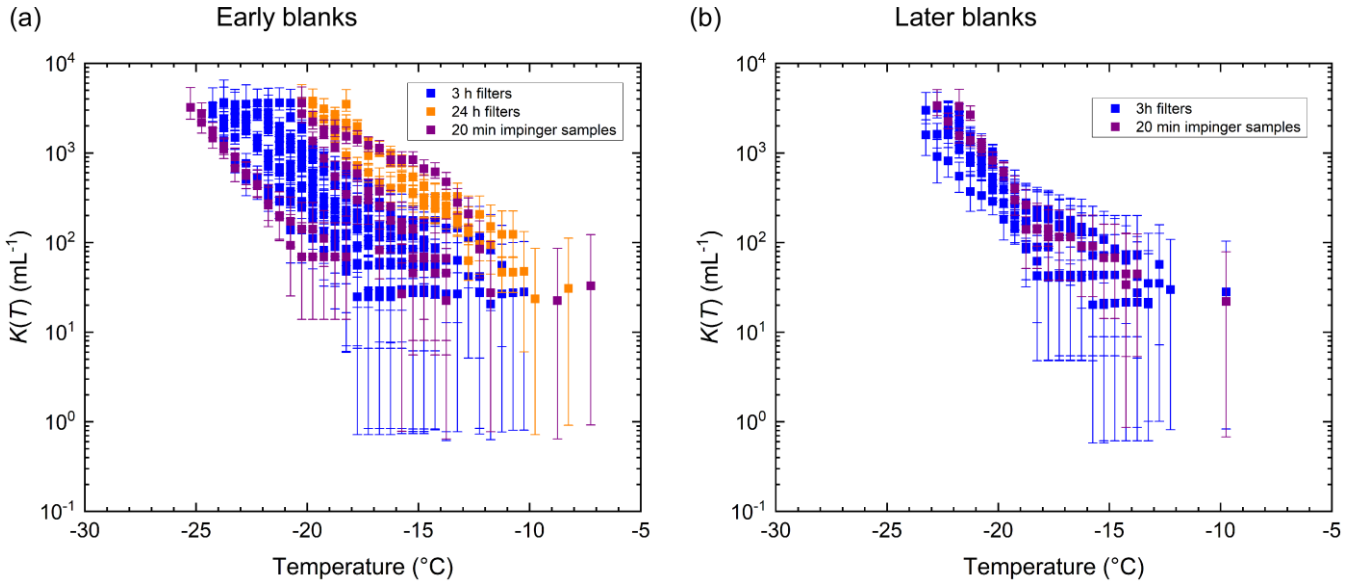

Figure S10: Plots showing background-corrected spectra for the samples in terms of the cumulative number of ice nucleation sites per unit volume of water, *K*(*T*), versus freezing temperature during the time periods for (a) the "early" blanks, and (b) the "later" blanks.

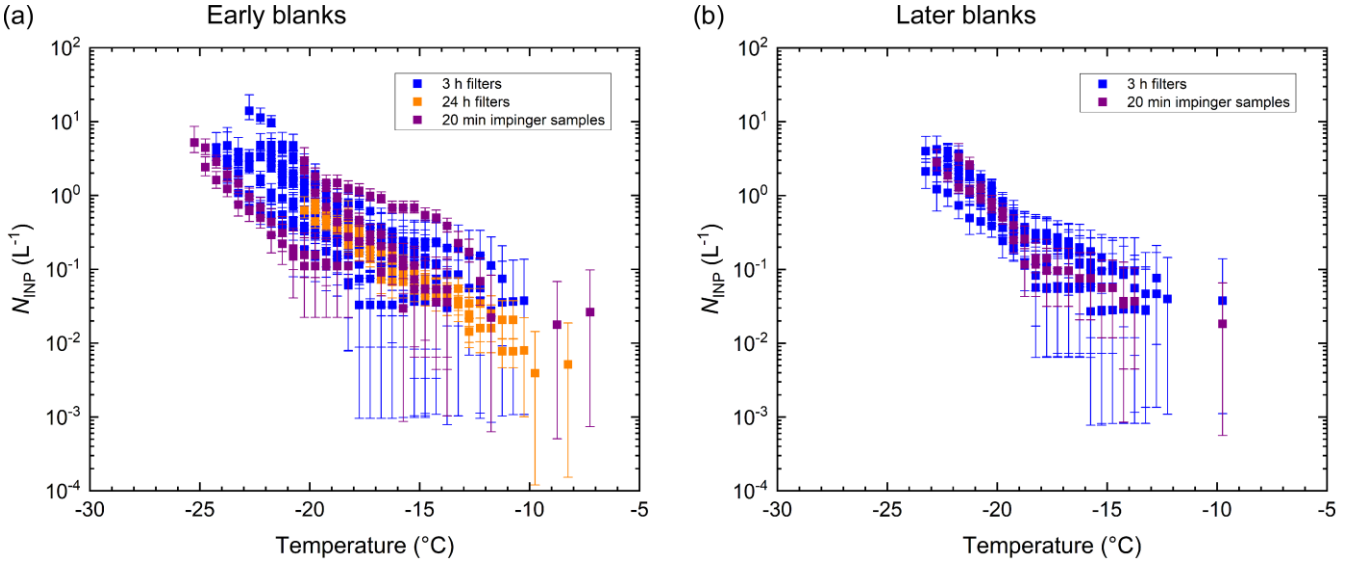

Figure S11: Plots showing the background-corrected ice-nucleating particle concentrations, N_{INP}, for all samples collected during the time periods for (a) the "early" blanks, and (b) the "later" blanks. Figure 1a in the main paper combines these plots together for the 3 h filter data, while the 24 h filter N_{INP} data and 20 min impinger N_{INP} data are shown individually below in Figure S12 and Figure S13, respectively.

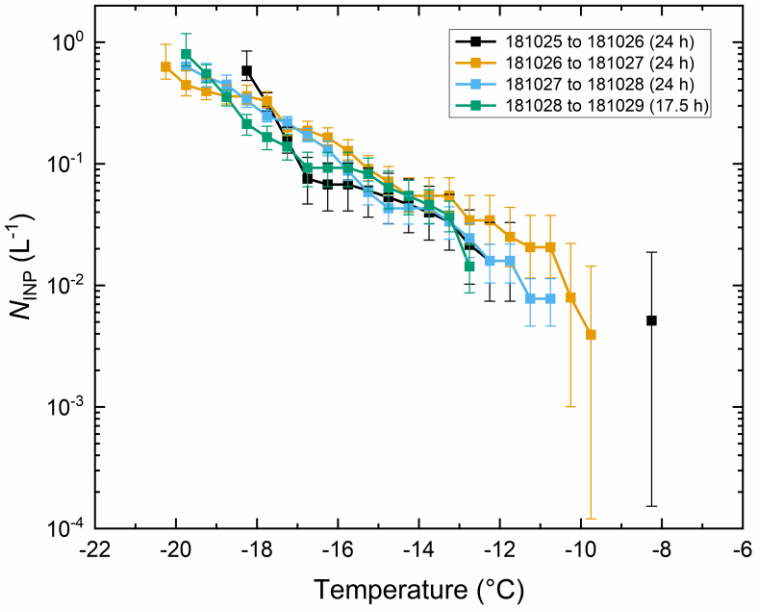

Figure S12: Plot of background-corrected ice-nucleating particle concentrations, N_{INP}, for samples collected onto filters for 24 h from 25th October to 29th October 2018, using a MesaLabs BGI PQ100 filter sampler with a PM_{10} inlet head. Lines represent the bulk of the data, with single droplets that froze at much warmer temperature shown as individual, unconnected data points. Dates are given in the YYMMDD format.

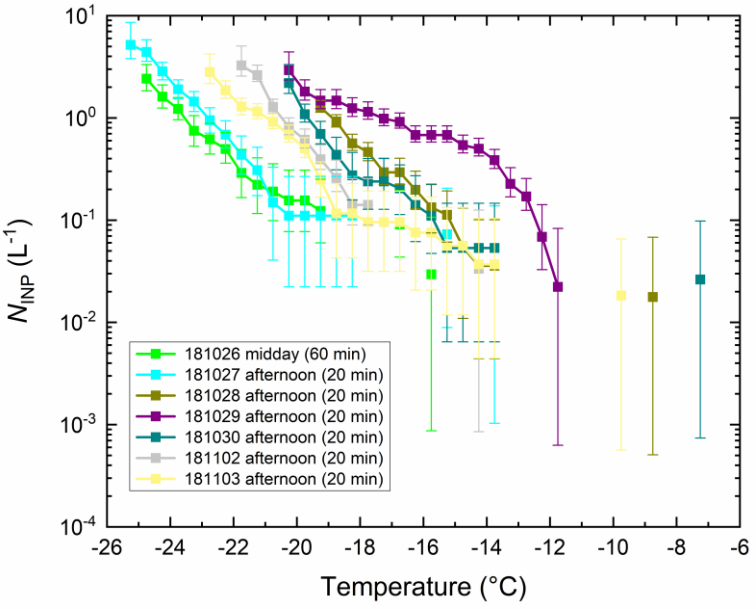

Figure S13: Plot of background-corrected ice-nucleating particle concentrations, N_{INP}, for samples collected using a Bertin Technologies Coriolis® Micro impinger for 20-40 min into <10 mL of purified water from 25th October-3rd November 2018. Lines and symbols are colour-coded to match those corresponding to the same timeframes (i.e. date and morning/afternoon) for the 3 h filter samples shown in Figure 1 in the main paper. Lines represent the bulk of the data, with single droplets that froze at much warmer temperature shown as individual, unconnected data points. Dates are given in the YYMMDD format.

7 Particle size distributions

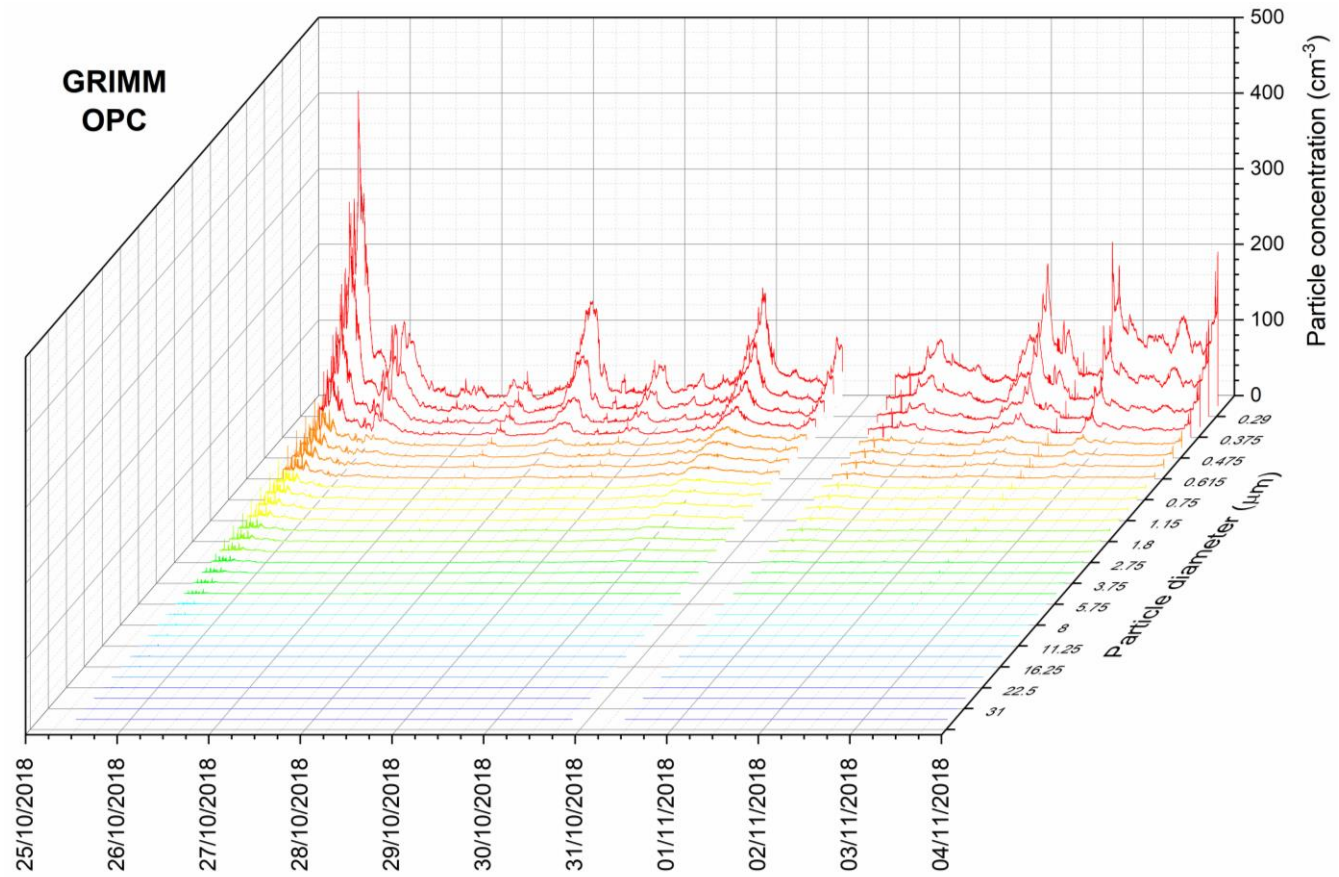

Figure S14: Time series showing the particle concentration (d*N*) data from throughout the campaign as measured by the GRIMM Model 1.109 optical particle counter (OPC; 0.25 – 32 µm particle diameter).

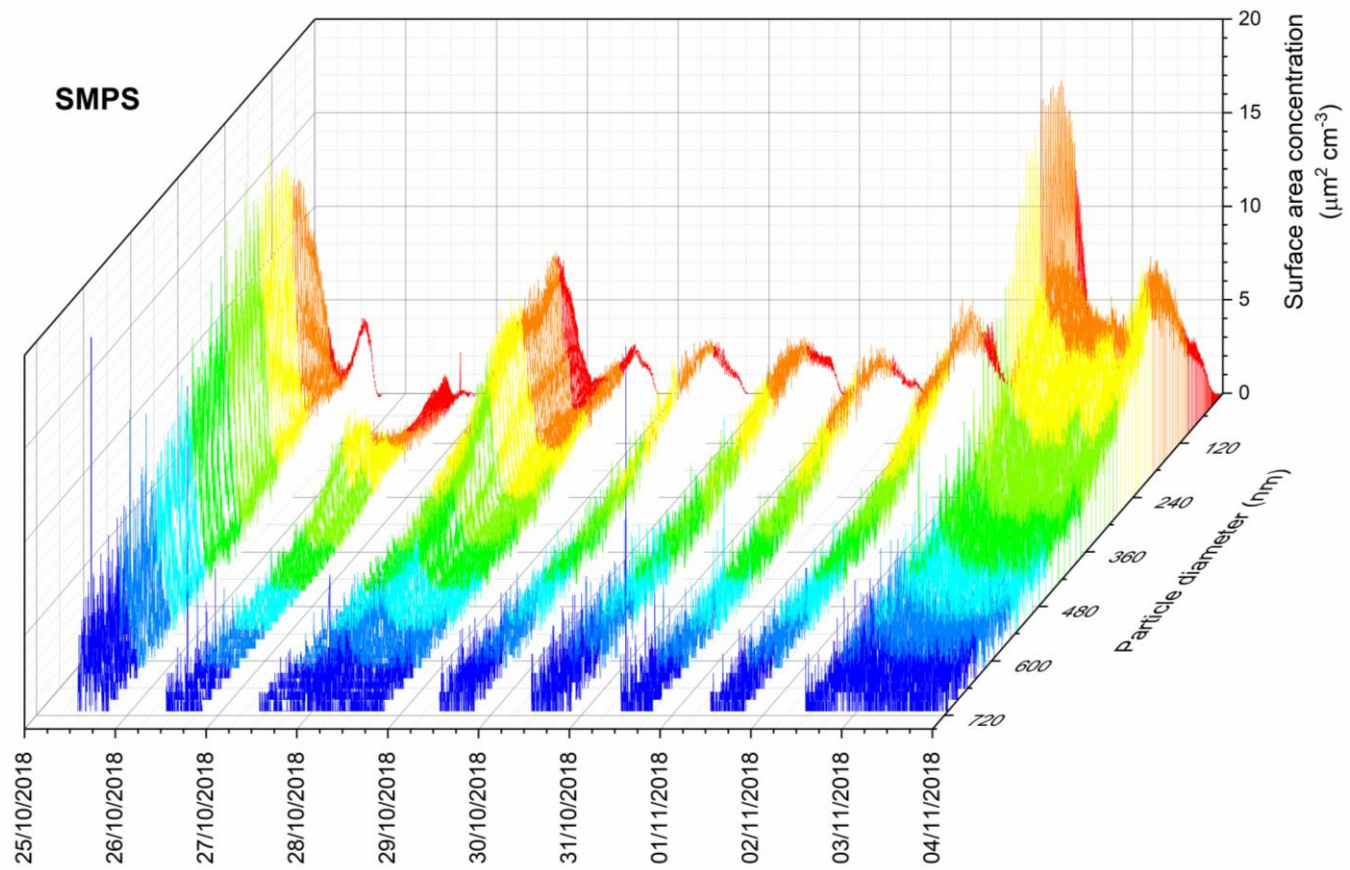

Figure S15: Time series showing the raw particle surface area concentration (d*S*) data from throughout the campaign as measured using the TSI Model 3938 scanning mobility particle sizer (SMPS) spectrometer (14.1 – 710.5 nm).

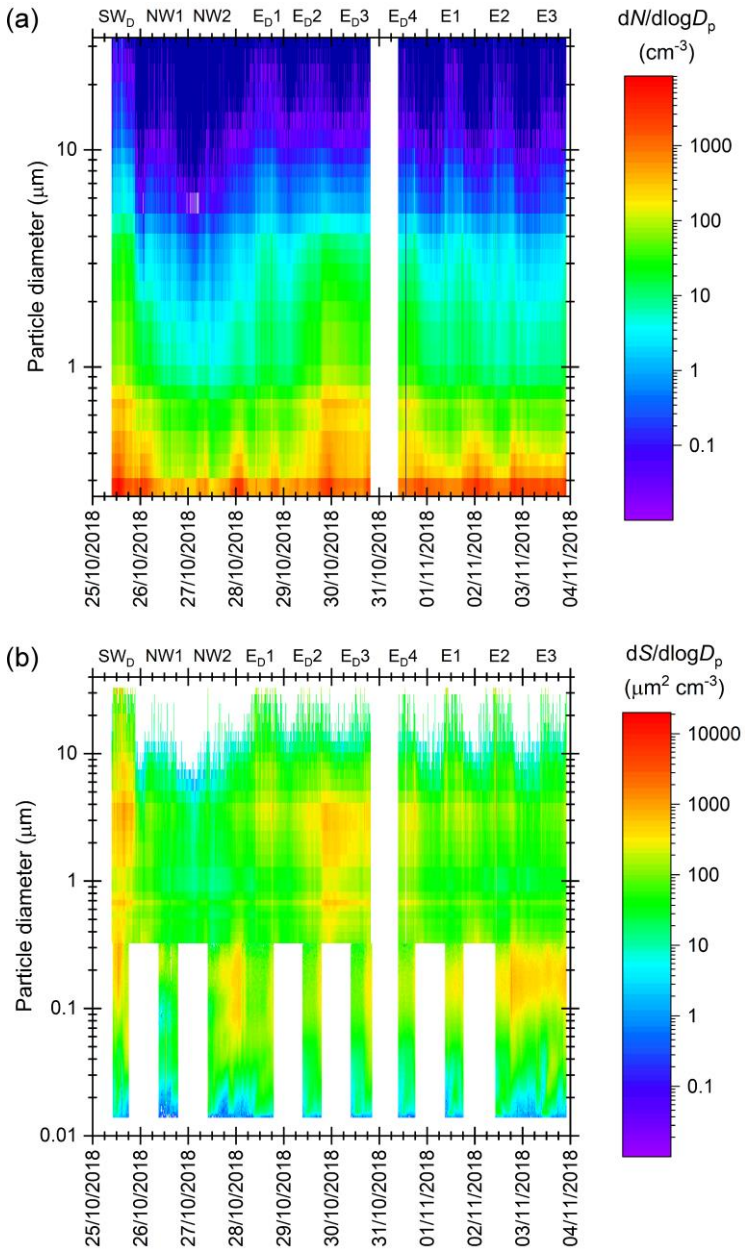

Figure S16: Time series showing particle size distributions throughout the campaign. (a) Particle diameter (D_p) versus normalised particle concentration (dN) in terms of dN/dlogD_p, as determined using the GRIMM OPC (0.25 – 32 µm). This figure is a higher resolution version of Figure 2h in the main paper. (b) Particle diameter (D_p) versus normalised particle surface area (dS) in terms of dS/dlogD_p, as determined by combining data obtained using both the SMPS (0.0141 – 0.322 µm) and the GRIMM OPC (0.325 – 31 µm). The values determined here were used to calculate the ice-active site surface density, $n_s(T)$. Air categories and IDs are given at the top of the plots.

8 Air mass back trajectories

210

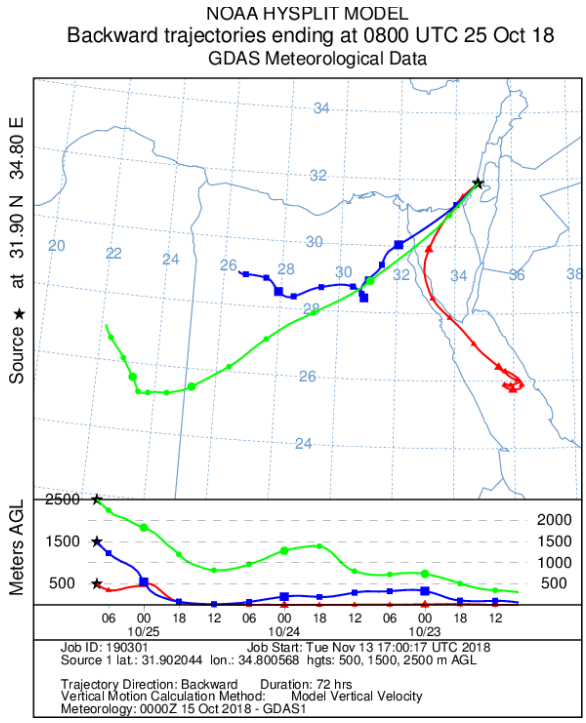

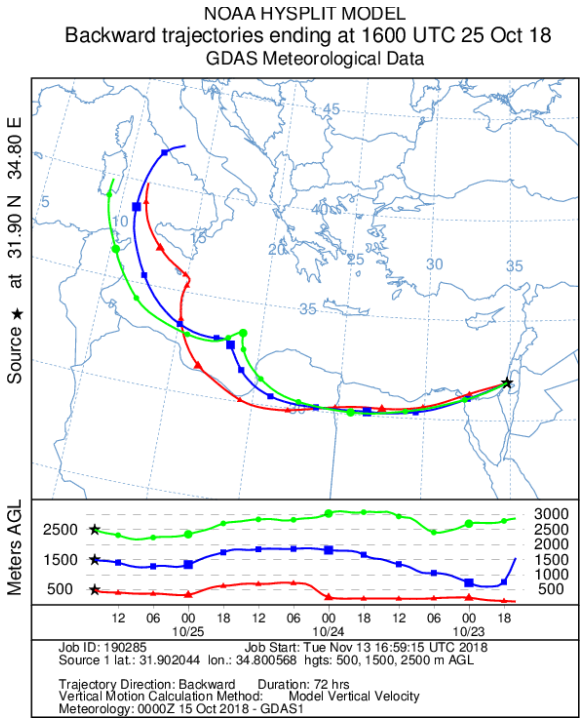

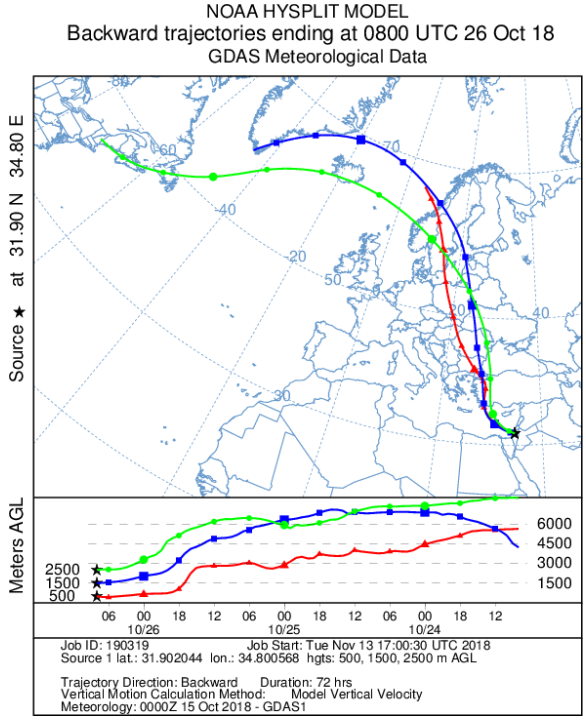

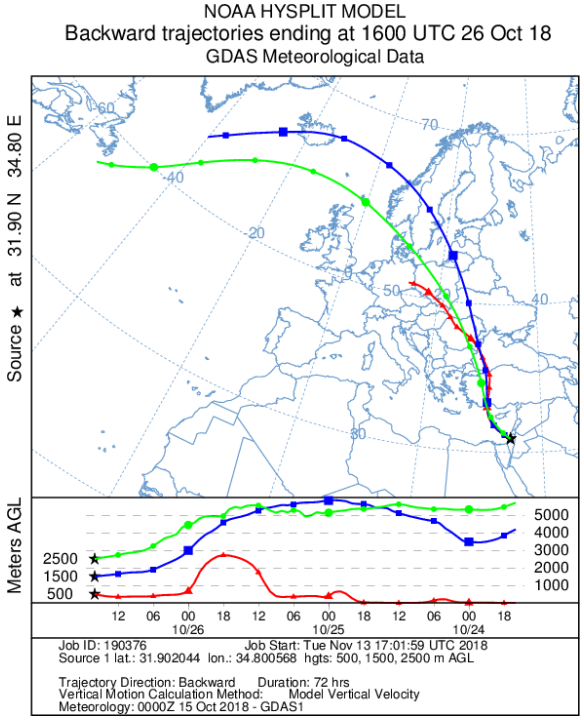

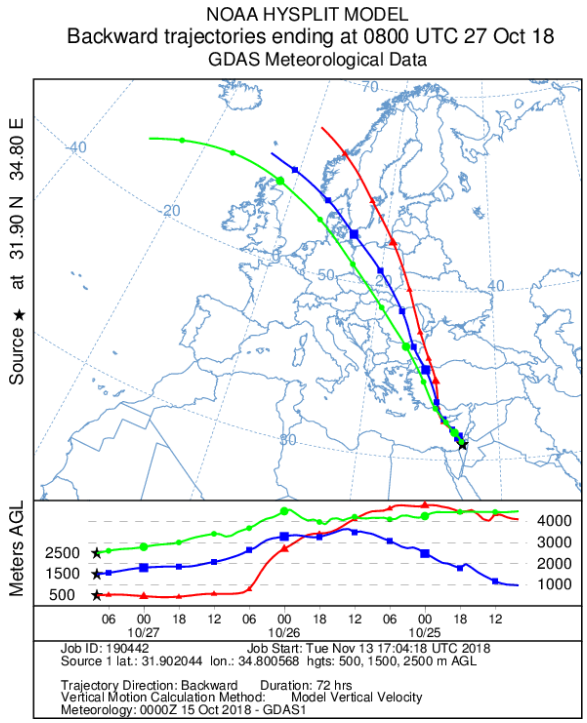
NOAA HYSPLIT MODEL
Backward trajectories ending at 0800 UTC 27 Oct 18
GDAS Meteorological Data
Source ★ at 31.90 N 34.80 E
Meters AGL
2500
1500
500
4000
3000
2000
1000
06 00 18 12 06 00 18 12 06 00 18 12
10/27 10/26 10/25
Job ID: 190442 Job Start: Tue Nov 13 17:04:18 UTC 2018
Source 1 lat.: 31.902044 lon.: 34.800568 hgts: 500, 1500, 2500 m AGL
Trajectory Direction: Backward Duration: 72 hrs
Vertical Motion Calculation Method: Model Vertical Velocity
Meteorology: 0000Z 15 Oct 2018 - GDAS1

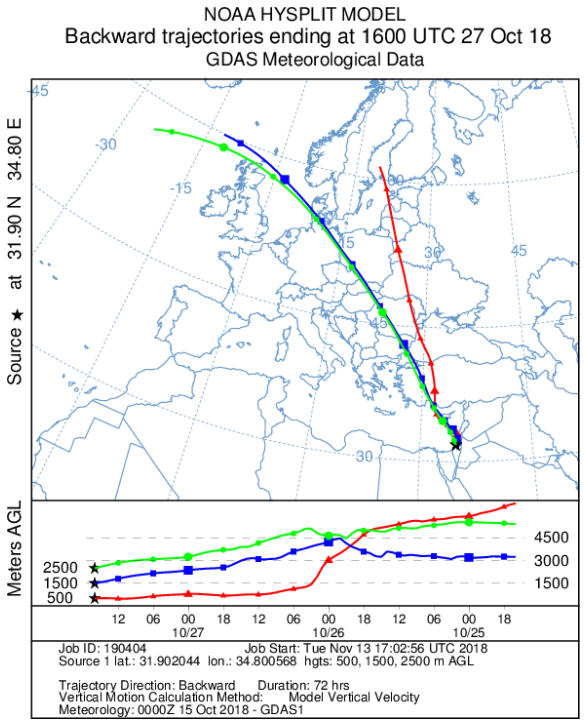
NOAA HYSPLIT MODEL
Backward trajectories ending at 1600 UTC 27 Oct 18
GDAS Meteorological Data
Source ★ at 31.90 N 34.80 E
Meters AGL
2500
1500
500
4500
3000
1500
12 06 00 18 12 06 00 18 12 06 00 18
10/27 10/26 10/25
Job ID: 190404 Job Start: Tue Nov 13 17:02:56 UTC 2018
Source 1 lat.: 31.902044 lon.: 34.800568 hgts: 500, 1500, 2500 m AGL
Trajectory Direction: Backward Duration: 72 hrs
Vertical Motion Calculation Method: Model Vertical Velocity
Meteorology: 0000Z 15 Oct 2018 - GDAS1

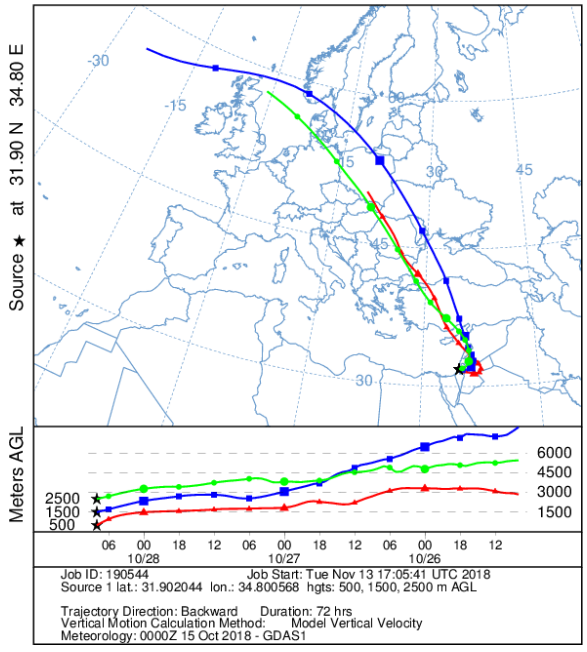
NOAA HYSPLIT MODEL
Backward trajectories ending at 0800 UTC 28 Oct 18
GDAS Meteorological Data
Source ★ at 31.90 N 34.80 E
Meters AGL
2500
1500
500
6000
4500
3000
1500
06 00 18 12 06 00 18 12 06 00 18 12
10/28 10/27 10/26
Job ID: 190544 Job Start: Tue Nov 13 17:05:41 UTC 2018
Source 1 lat.: 31.902044 lon.: 34.800568 hgts: 500, 1500, 2500 m AGL
Trajectory Direction: Backward Duration: 72 hrs
Vertical Motion Calculation Method: Model Vertical Velocity
Meteorology: 0000Z 15 Oct 2018 - GDAS1

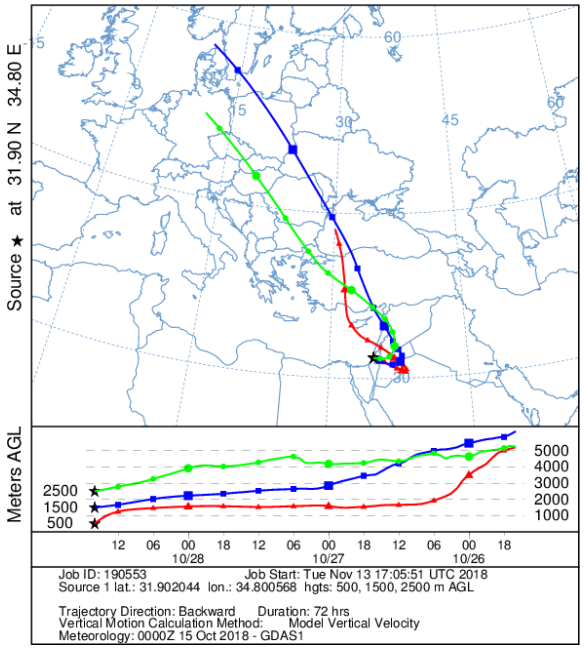
NOAA HYSPLIT MODEL
Backward trajectories ending at 1600 UTC 28 Oct 18
GDAS Meteorological Data
Source ★ at 31.90 N 34.80 E
Meters AGL
2500
1500
500
5000
4000
3000
2000
1000
12 06 00 18 12 06 00 18 12 06 00 18
10/28 10/27 10/26
Job ID: 190553 Job Start: Tue Nov 13 17:05:51 UTC 2018
Source 1 lat.: 31.902044 lon.: 34.800568 hgts: 500, 1500, 2500 m AGL
Trajectory Direction: Backward Duration: 72 hrs
Vertical Motion Calculation Method: Model Vertical Velocity
Meteorology: 0000Z 15 Oct 2018 - GDAS1

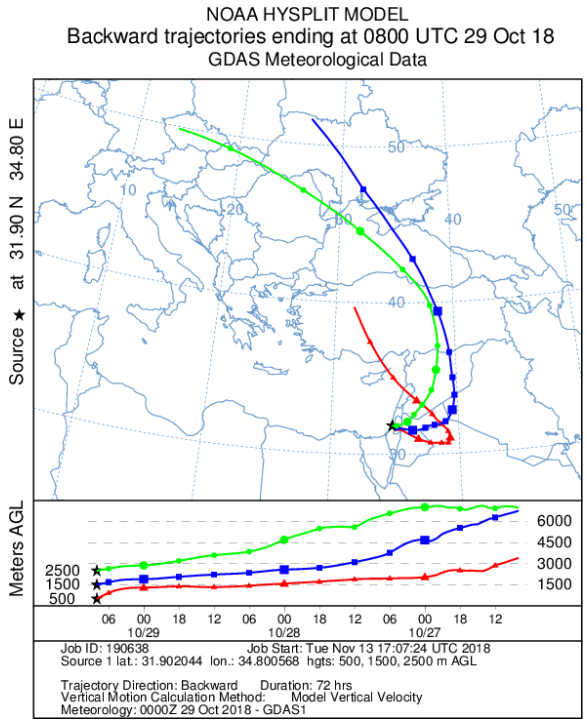
NOAA HYSPLIT MODEL
Backward trajectories ending at 0800 UTC 29 Oct 18
GDAS Meteorological Data
Source ★ at 31.90 N 34.80 E
Meters AGL
2500
1500
500
6000
4500
3000
1500
06 00 18 12 06 00 18 12 06 00 18 12
10/29 10/28 10/27
Job ID: 190638 Job Start: Tue Nov 13 17:07:24 UTC 2018
Source 1 lat.: 31.902044 lon.: 34.800568 hgts: 500, 1500, 2500 m AGL
Trajectory Direction: Backward Duration: 72 hrs
Vertical Motion Calculation Method: Model Vertical Velocity
Meteorology: 0000Z 29 Oct 2018 - GDAS1

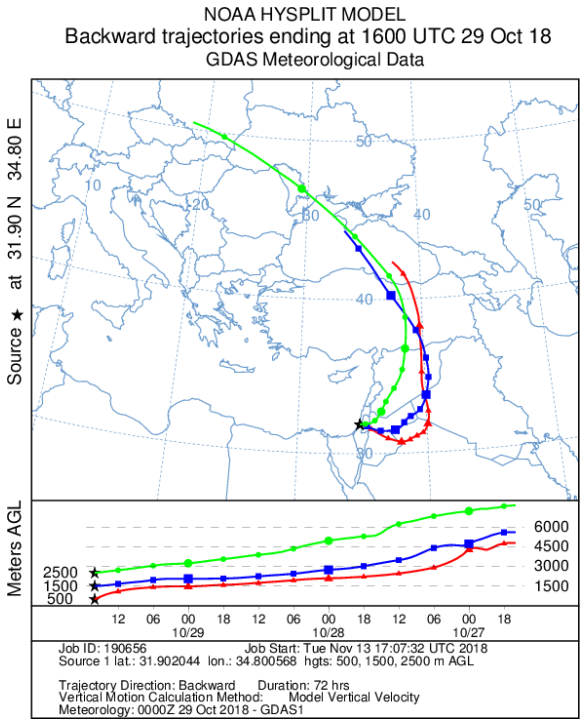
NOAA HYSPLIT MODEL
Backward trajectories ending at 1600 UTC 29 Oct 18
GDAS Meteorological Data
Source ★ at 31.90 N 34.80 E
Meters AGL
2500
1500
500
6000
4500
3000
1500
12 06 00 18 12 06 00 18 12 06 00 18
10/29 10/28 10/27
Job ID: 190656 Job Start: Tue Nov 13 17:07:32 UTC 2018
Source 1 lat.: 31.902044 lon.: 34.800568 hgts: 500, 1500, 2500 m AGL
Trajectory Direction: Backward Duration: 72 hrs
Vertical Motion Calculation Method: Model Vertical Velocity
Meteorology: 0000Z 29 Oct 2018 - GDAS1

215

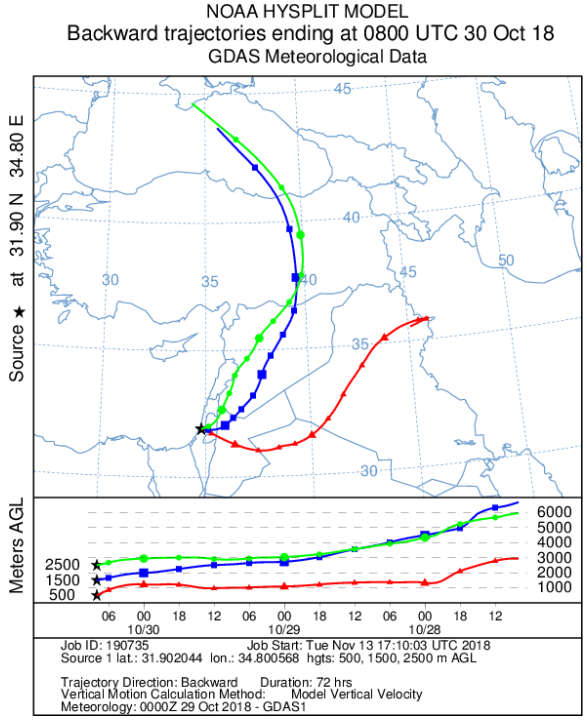
NOAA HYSPLIT MODEL
Backward trajectories ending at 0800 UTC 30 Oct 18
GDAS Meteorological Data
Source ★ at 31.90 N 34.80 E
Meters AGL
2500
1500
500
6000
5000
4000
3000
2000
1000
06 00 18 12 06 00 18 12 06 00 18 12
10/30 10/29 10/28
Job ID: 190735 Job Start: Tue Nov 13 17:10:03 UTC 2018
Source 1 lat.: 31.902044 lon.: 34.800568 hgts: 500, 1500, 2500 m AGL
Trajectory Direction: Backward Duration: 72 hrs
Vertical Motion Calculation Method: Model Vertical Velocity
Meteorology: 0000Z 29 Oct 2018 - GDAS1

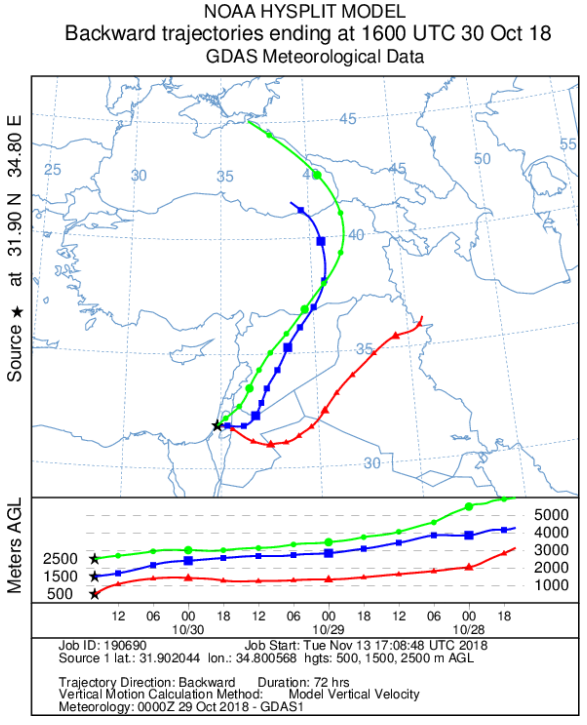
NOAA HYSPLIT MODEL
Backward trajectories ending at 1600 UTC 30 Oct 18
GDAS Meteorological Data
Source ★ at 31.90 N 34.80 E
Meters AGL
2500
1500
500
5000
4000
3000
2000
1000
12 06 00 18 12 06 00 18 12 06 00 18
10/30 10/29 10/28
Job ID: 190690 Job Start: Tue Nov 13 17:08:48 UTC 2018
Source 1 lat.: 31.902044 lon.: 34.800568 hgts: 500, 1500, 2500 m AGL
Trajectory Direction: Backward Duration: 72 hrs
Vertical Motion Calculation Method: Model Vertical Velocity
Meteorology: 0000Z 29 Oct 2018 - GDAS1

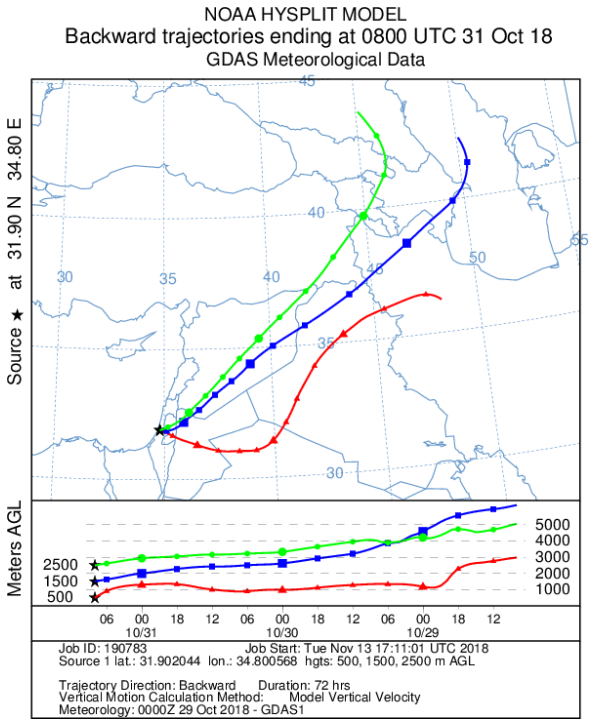
NOAA HYSPLIT MODEL
Backward trajectories ending at 0800 UTC 31 Oct 18
GDAS Meteorological Data
Source ★ at 31.90 N 34.80 E
Meters AGL
2500
1500
500
5000
4000
3000
2000
1000
06 00 18 12 06 00 18 12 06 00 18 12
10/31 10/30 10/29
Job ID: 190783 Job Start: Tue Nov 13 17:11:01 UTC 2018
Source 1 lat.: 31.902044 lon.: 34.800568 hgts: 500, 1500, 2500 m AGL
Trajectory Direction: Backward Duration: 72 hrs
Vertical Motion Calculation Method: Model Vertical Velocity
Meteorology: 0000Z 29 Oct 2018 - GDAS1

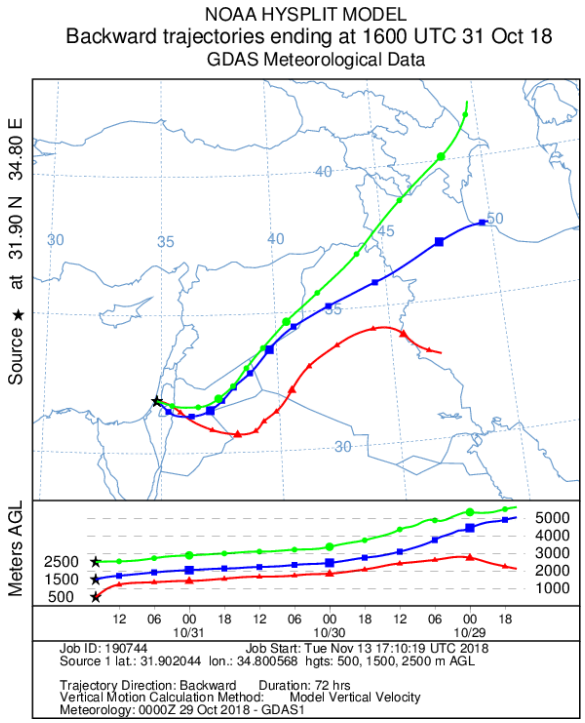
NOAA HYSPLIT MODEL
Backward trajectories ending at 1600 UTC 31 Oct 18
GDAS Meteorological Data
Source ★ at 31.90 N 34.80 E
Meters AGL
2500
1500
500
5000
4000
3000
2000
1000
12 06 00 18 12 06 00 18 12 06 00 18
10/31 10/30 10/29
Job ID: 190744 Job Start: Tue Nov 13 17:10:19 UTC 2018
Source 1 lat.: 31.902044 lon.: 34.800568 hgts: 500, 1500, 2500 m AGL
Trajectory Direction: Backward Duration: 72 hrs
Vertical Motion Calculation Method: Model Vertical Velocity
Meteorology: 0000Z 29 Oct 2018 - GDAS1

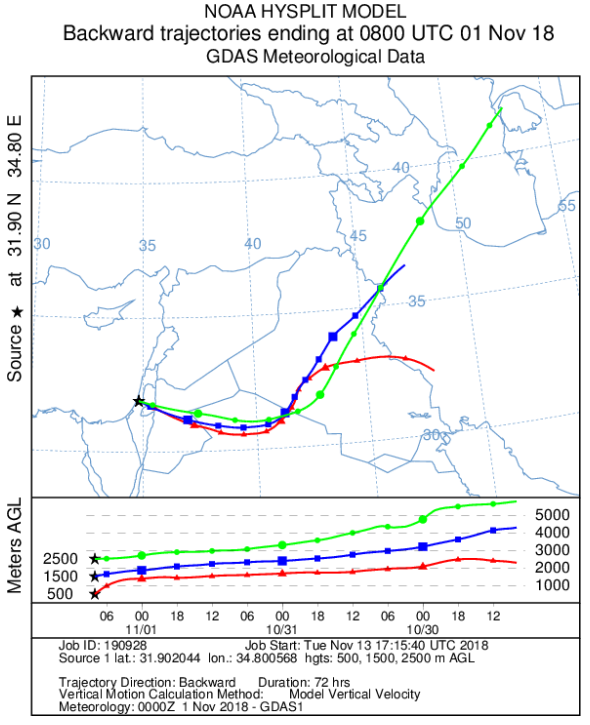
NOAA HYSPLIT MODEL
Backward trajectories ending at 0800 UTC 01 Nov 18
GDAS Meteorological Data
Source ★ at 31.90 N 34.80 E
Meters AGL
2500
1500
500
5000
4000
3000
2000
1000
06 00 18 12 06 00 18 12 06 00 18 12
11/01 10/31 10/30
Job ID: 190928 Job Start: Tue Nov 13 17:15:40 UTC 2018
Source 1 lat.: 31.902044 lon.: 34.800568 hgts: 500, 1500, 2500 m AGL
Trajectory Direction: Backward Duration: 72 hrs
Vertical Motion Calculation Method: Model Vertical Velocity
Meteorology: 0000Z 1 Nov 2018 - GDAS1

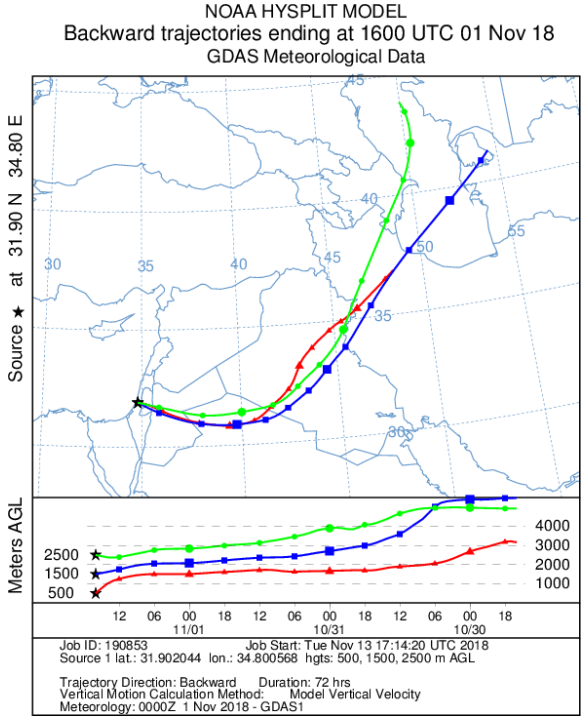
NOAA HYSPLIT MODEL
Backward trajectories ending at 1600 UTC 01 Nov 18
GDAS Meteorological Data
Source ★ at 31.90 N 34.80 E
Meters AGL
2500
1500
500
4000
3000
2000
1000
12 06 00 18 12 06 00 18 12 06 00 18
11/01 10/31 10/30
Job ID: 190853 Job Start: Tue Nov 13 17:14:20 UTC 2018
Source 1 lat.: 31.902044 lon.: 34.800568 hgts: 500, 1500, 2500 m AGL
Trajectory Direction: Backward Duration: 72 hrs
Vertical Motion Calculation Method: Model Vertical Velocity
Meteorology: 0000Z 1 Nov 2018 - GDAS1

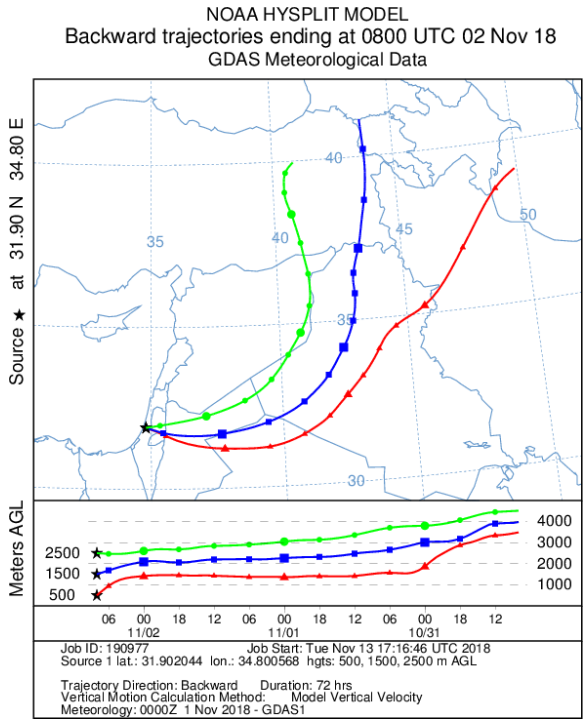
NOAA HYSPLIT MODEL
Backward trajectories ending at 0800 UTC 02 Nov 18
GDAS Meteorological Data
Source ★ at 31.90 N 34.80 E
Meters AGL
Job ID: 190977 Job Start: Tue Nov 13 17:16:46 UTC 2018
Source 1 lat.: 31.902044 lon.: 34.800568 hgts: 500, 1500, 2500 m AGL
Trajectory Direction: Backward Duration: 72 hrs
Vertical Motion Calculation Method: Model Vertical Velocity
Meteorology: 0000Z 1 Nov 2018 - GDAS1

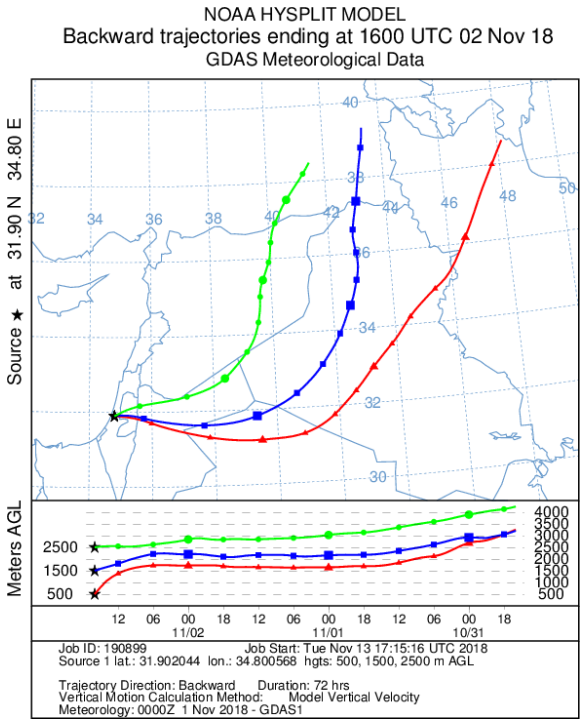
NOAA HYSPLIT MODEL
Backward trajectories ending at 1600 UTC 02 Nov 18
GDAS Meteorological Data
Source ★ at 31.90 N 34.80 E
Meters AGL
Job ID: 190899 Job Start: Tue Nov 13 17:15:16 UTC 2018
Source 1 lat.: 31.902044 lon.: 34.800568 hgts: 500, 1500, 2500 m AGL
Trajectory Direction: Backward Duration: 72 hrs
Vertical Motion Calculation Method: Model Vertical Velocity
Meteorology: 0000Z 1 Nov 2018 - GDAS1

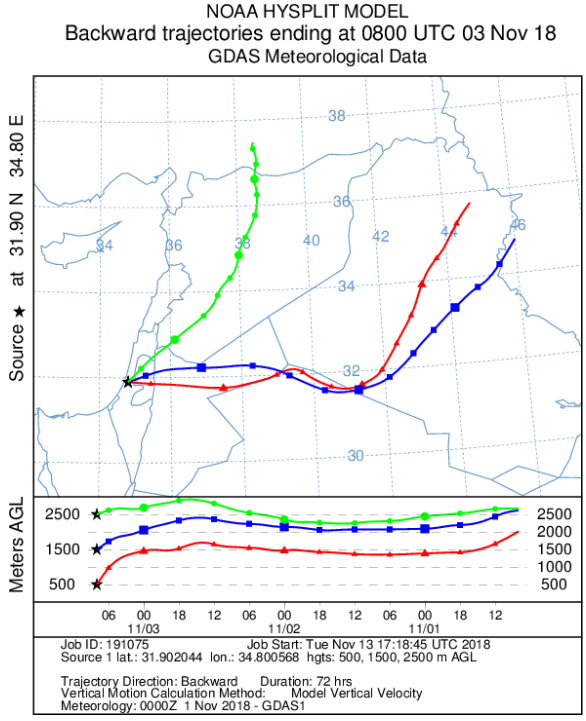
NOAA HYSPLIT MODEL
Backward trajectories ending at 0800 UTC 03 Nov 18
GDAS Meteorological Data
Source ★ at 31.90 N 34.80 E
Meters AGL
Job ID: 191075 Job Start: Tue Nov 13 17:18:45 UTC 2018
Source 1 lat.: 31.902044 lon.: 34.800568 hgts: 500, 1500, 2500 m AGL
Trajectory Direction: Backward Duration: 72 hrs
Vertical Motion Calculation Method: Model Vertical Velocity
Meteorology: 0000Z 1 Nov 2018 - GDAS1

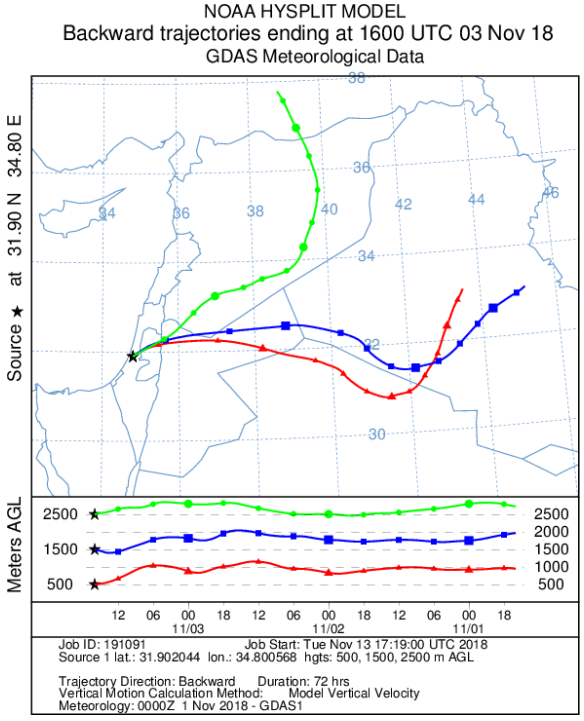
NOAA HYSPLIT MODEL
Backward trajectories ending at 1600 UTC 03 Nov 18
GDAS Meteorological Data
Source ★ at 31.90 N 34.80 E
Meters AGL
Job ID: 191091 Job Start: Tue Nov 13 17:19:00 UTC 2018
Source 1 lat.: 31.902044 lon.: 34.800568 hgts: 500, 1500, 2500 m AGL
Trajectory Direction: Backward Duration: 72 hrs
Vertical Motion Calculation Method: Model Vertical Velocity
Meteorology: 0000Z 1 Nov 2018 - GDAS1

220

Figure S17: Air mass back trajectories (72 h) determined using the National Oceanic and Atmospheric Administration (NOAA) Air Resources Laboratory's HYSPLIT (Hybrid Single Particle Lagrangian Integrated Trajectory) model (https://www.arl.noaa.gov/hysplit/) (Stein et al., 2016) throughout the campaign. The left column represents air masses reaching Israel (represented by a star) in the mornings while the right column represents air masses reaching in the afternoons. Times are in UTC (Coordinated Universal Time), while time in Israel is UTC+2, hence the end times for the air masses in the left column are 10:00 local time in Israel (08:00 UTC) and the end times in the right column are at 18:00 local time (16:00 UTC). Above ground level (AGL) altitudes of 500 m are shown in red, 1500 m are shown in blue, and 2500 m are shown in green.

9 PM_{10} vs. PM_1 for "181029 afternoon"

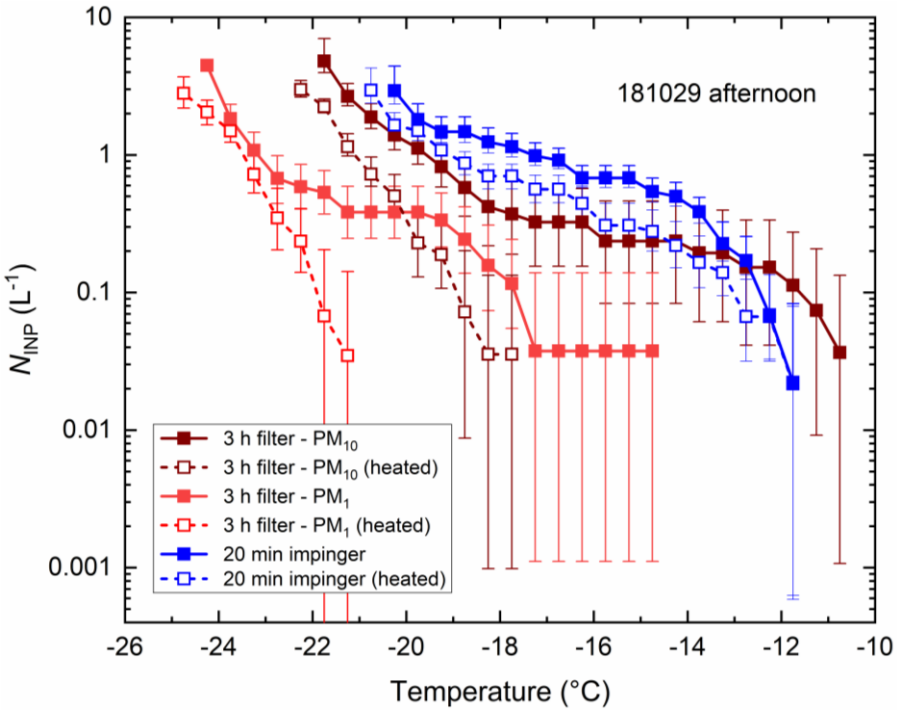

Figure S18: Background-corrected ice-nucleating particle concentrations, N_{INP}, for 3 h filter samples collected simultaneously using PM_{10} and PM_1 inlet heads on two MesaLabs PQ100 air sampling systems on the afternoon of 29th October 2018. A sample collected within the same time period for 20 min using Bertin Technologies Coriolis® Micro air sampler impinger sampler is also shown. All samples were subjected to heat treatment (95 °C for 30 min) to test for potential proteinaceous INPs, as per Daily et al. (2022), and those results are also shown here. The date in the figure is in the YYMMDD format.

10 Heat treatments

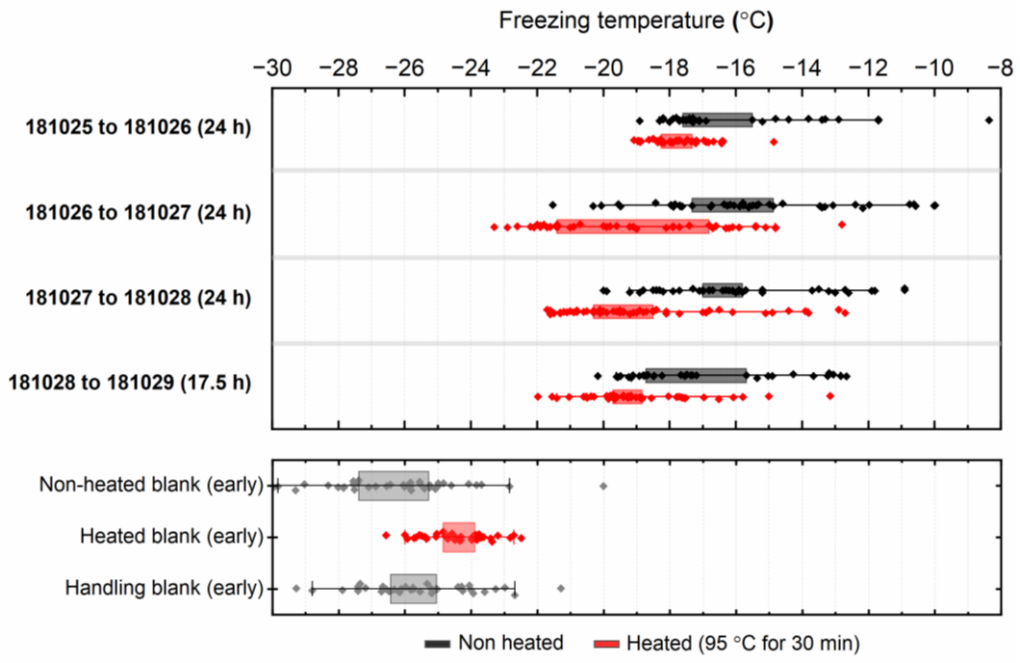

Figure S19: Box-and-whisker plots showing the effect of heat treatment (95 °C for 30 min, as per Daily et al. (2022)) on the ice-nucleating activity of aqueous particle suspensions obtained from 24 h filter samples as an indicator of potential proteinaceous INPs. Heat treatments of heated and non-heated purified water "early" blanks as control tests are provided, in addition to an "early" handling blank obtained using a HEPA filter. Boxes represent 1 standard deviation from the mean (1σ; 68 %) while whiskers represent 2 standard deviations (2σ; 95 %). Dates are given in the DD/MM/YY format.

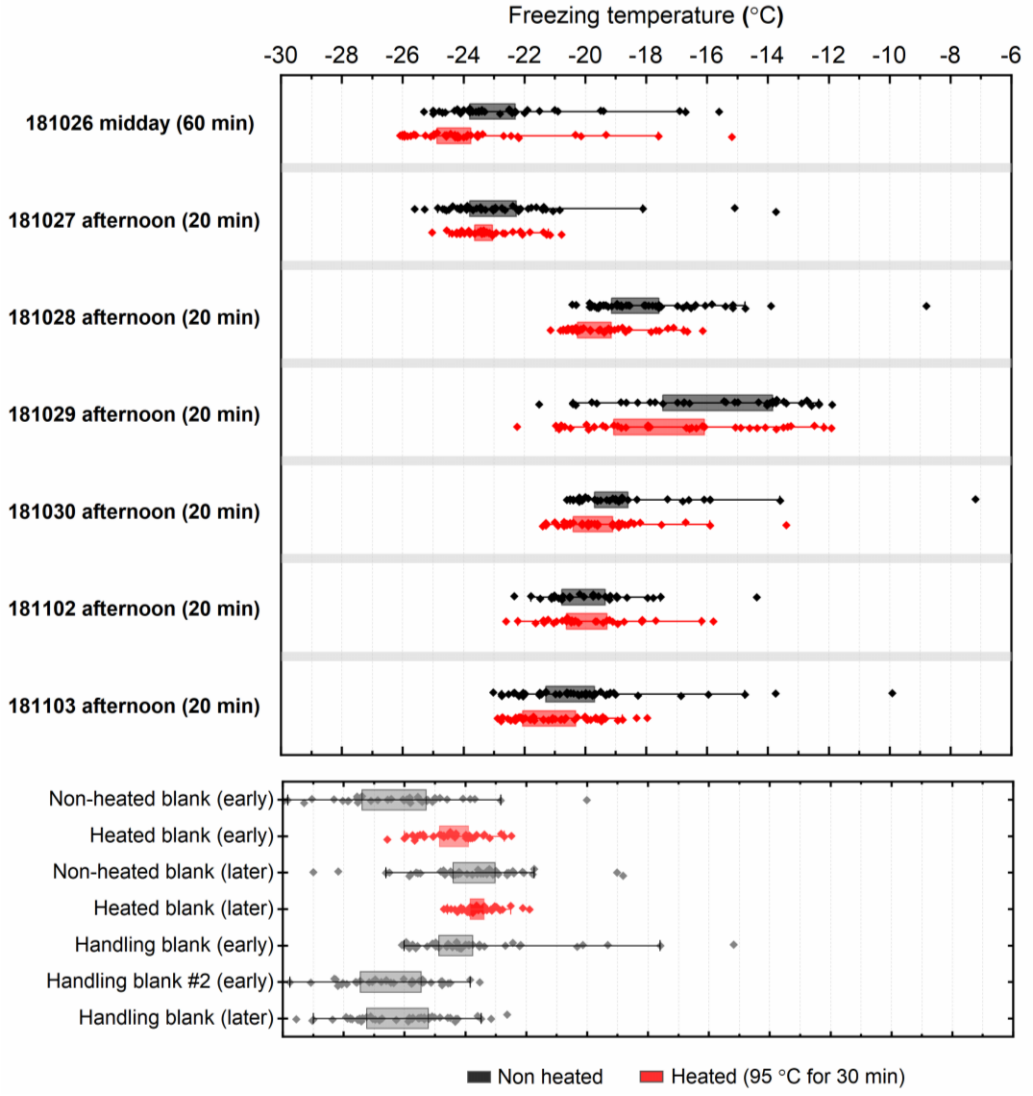

Figure S20: Box-and-whisker plots showing the effect of heat treatment (95 °C for 30 min, as per Daily et al. (2022)) on the ice-nucleating activity of aqueous particle suspensions obtained from 20-40 min impinger samples as an indicator of potential proteinaceous INPs. Heat treatments of heated and non-heated purified water blanks as control tests are provided for both "early" and "late" blanks alongside data for non-heated handling blanks. Boxes represent 1 standard deviation from the mean (1σ; 68 %) while whiskers represent 2 standard deviations (2σ; 95 %). Dates are given in the DD/MM/YY format.

11 Data availability

The data sets for this article will be made publicly available in the University of Leeds Data Repository (https://archive.researchdata.leeds.ac.uk/).

12 References

Bräuer, S. L., Adams, C., Kranzler, K., Murphy, D., Xu, M., Zuber, P., Simon, H. M., Baptista, A. M., and Tebo, B. M.: Culturable Rhodobacter and Shewanella species are abundant in estuarine turbidity maxima of the Columbia River, Environ. Microbiol., 13, 589-603, https://doi.org/10.1111/j.1462-2920.2010.02360.x, 2011.

Daily, M. I., Tarn, M. D., Whale, T. F., and Murray, B. J.: An evaluation of the heat test for the ice-nucleating ability of minerals and biological material, Atmos. Meas. Tech., 15, 2635-2665, https://doi.org/10.5194/amt-15-2635-2022, 2022.

Gat, D., Reicher, N., Schechter, S., Alayof, M., Tarn, M. D., Wyld, B. V., Zimmermann, R., and Rudich, Y.: Size-Resolved Community Structure of Bacteria and Fungi Transported by Dust in the Middle East, 12, https://doi.org/10.3389/fmicb.2021.744117, 2021.

Harrison, A. D., O'Sullivan, D., Adams, M. P., Porter, G. C. E., Blades, E., Brathwaite, C., Chewitt-Lucas, R., Gaston, C., Hawker, R., Krüger, O. O., Neve, L., Pöhlker, M. L., Pöhlker, C., Pöschl, U., Sanchez-Marroquin, A., Sealy, A., Sealy, P., Tarn, M. D., Whitehall, S., McQuaid, J. B., Carslaw, K. S., Prospero, J. M., and Murray, B. J.: The ice-nucleating activity of African mineral dust in the Caribbean boundary layer, Atmos. Chem. Phys., 22, 9663-9680, https://doi.org/10.5194/acp-22-9663-2022, 2022.

Krasnov, H., Katra, I., and Friger, M.: Increase in dust storm related PM10 concentrations: A time series analysis of 2001–2015, Environmental Pollution, 213, 36-42, https://doi.org/10.1016/j.envpol.2015.10.021, 2016.

Stein, A. F., Draxler, R. R., Rolph, G. D., Stunder, B. J. B., Cohen, M. D., and Ngan, F.: NOAA's HYSPLIT Atmospheric Transport and Dispersion Modeling System, Bulletin of the American Meteorological Society, 96, 2059-2077, https://doi.org/10.1175/bams-d-14-00110.1, 2016.

Vali, G.: Revisiting the differential freezing nucleus spectra derived from drop-freezing experiments: methods of calculation, applications, and confidence limits, Atmos. Meas. Tech., 12, 1219-1231, https://doi.org/10.5194/amt-12-1219-2019, 2019.

White, T. J., Bruns, T. D., Lee, S. B., and Taylor, J. W.: Amplification and Direct Sequencing of Fungal Ribosomal RNA Genes for Phylogenetics, in: PCR Protocols, Edited by: Innis, M. A., Gelfand, D. H., Sninsky, J. J., and White, T. J., Academic Press, San Diego, 315-322, 1990.